Dynamics of drops in branched tubes

By MICHAEL MANGA†

Department of Geology & Geophysics, University of California, Berkeley, CA 94720, USA

The flow of two-dimensional deformable drops through branching (bifurcating) tubes is studied numerically using a boundary integral formulation. The undeformed drop diameter is assumed to be less than the tube diameter. Capillary numbers between 10^{-2} and 1 are considered. Flow in the branching tube is characterized by the fraction of fluid which enters each of the two downstream branches. The likelihood of drops entering the high-flow-rate branch increases as (i) the viscosity ratio between the drops and suspending fluid decreases, (ii) the capillary number increases, and (iii) the drop size increases. Hydrodynamic interactions between the suspended drops increase the number of drops which enter the low-flow-rate branch. The implications of these results for dispersion processes and local transport are explored. The disturbance flow created by drops passing over 'dead-end' pores or cavities results in fluid transfer between the pore and the free stream; suspensions may then be effective in improving the 'cleaning' of porous materials.

1. Introduction

The flow of two or more immiscible fluids in a porous material occurs during the subsurface cleanup of organic contaminants, within oil reservoirs during oil and gas extraction, as well as in separation processes such as filtration. The non-wetting phase typically exists in the form of dispersed drops for volumes fractions of less than about 20%. Here we study the motion of drops in branching tubes as a model for the flow of two immiscible fluids in a porous medium, and consider the limits in which the dispersed phase occurs in the form of drops with undeformed radii less than the tube radius. The geometry of the model problem is also characteristic of the motion of blood cells in branching capillaries.

Consider a porous medium containing two immiscible fluids, as illustrated in figure 1. In order to develop both a qualitative and quantitative understanding of the dynamics which characterize the porous medium, studies focusing on length scales of the individual pores have considered three classes of model problems: the motion of a drop through a straight capillary, the motion and breakup of a drop passing through a contraction in a capillary, and finally, the motion of a drop through a branched capillary. These three model problems simulate drop–wall interactions, changes in pore dimensions, and bifurcations of flow pathways, respectively. The overall goal of these studies has been to develop models which characterize macrophysical properties of the two-phase system, such as the effective viscosity, texture of the dispersed phase, and mechanical dispersion, in terms of microphysical properties such as drop size, the capillary number (relative magnitude of viscous to interfacial tension forces

† Present address: Department of Geological Sciences, University of Oregon, Eugene, OR 97403, USA.
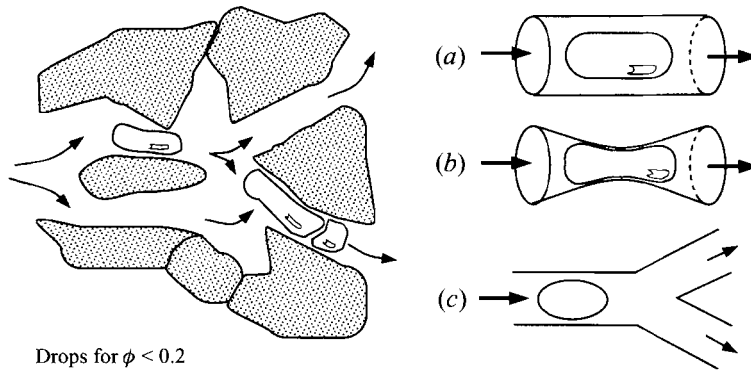
FIGURE 1. Schematic illustration of droplets (dispersed non-wetting phase) in a porous material; ϕ is volume fraction of the dispersed phase (compared with the volume of the suspending fluid). Owing to the geometric complexity of typical porous materials, three model problems are often studied: (*a*) a drop in a straight capillary, (*b*) a drop in a constricted capillary, and (*c*) a drop in a branched capillary. This paper considers a two-dimensional version of model geometry (*c*).

acting on the drop), and the viscosity ratio between the drop and surrounding fluid. For example, analytical (e.g. Bretherton 1961; Brenner 1971; Ratulowski & Chang 1989), numerical (e.g. Martinez & Udell 1990), and experimental (e.g. Ho & Leal 1975) studies of a single drop in a straight capillary have determined the relationship between the pressure change across the drop and the relative drop size, the viscosity ratio and the drop velocity, so that a model for the effective viscosity of the two-phase system can be developed. While the model problems illustrated in figure 1(*a–c*) are obviously greatly simplified models of an actual porous medium in which a variety of physicochemical processes may influence drop dynamics, the model problems do provide a starting point for studying certain pore-scale processes.

A recent summary of research on drops and bubbles in straight and constricted capillaries, model problems (*a*) and (*b*) in figure 1, may be found in Tsai & Miksis (1994). Here we study drop motion in branched tubes (figure 1*c*) in order to study the effect of bifurcations on the motion of drops and the effect of drops on the local transport of passive tracers. Similar calculations for two-dimensional rigid particles have been presented by Audet & Olbricht (1987) and related low Reynolds number experimental work for two interacting rigid particles has been performed by Ditchfield & Olbricht (1995). Other numerical work includes lattice-Boltzman numerical simulations which allow very complex three-dimensional porous structures to be studied (e.g. Gunstensen & Rothman 1993; Adler 1992). While the relevant geometry is three-dimensional, owing to numerical limitations we will consider a two-dimensional model. A comparison of analytical (e.g. Chan & Leal 1979) and numerical (e.g. Zhou & Pozrikidis 1994) studies indicates that while certain quantitative differences exist between the motion and deformation of two-dimensional and three-dimensional neutrally buoyant drops in tubes and channels, qualitative features of the problem are largely unaffected. Although the two-dimensional approximation may restrict direct quantitative applications of the results, the simplifying assumption does allow us to perform a numerical study and consider the effects of drop size, viscosity ratio, geometry, and drop interactions on the motion of drops through branching tubes, and thus to develop at least a qualitative understanding of the problem.†

† The author can provide animated videos of the calculations presented here.
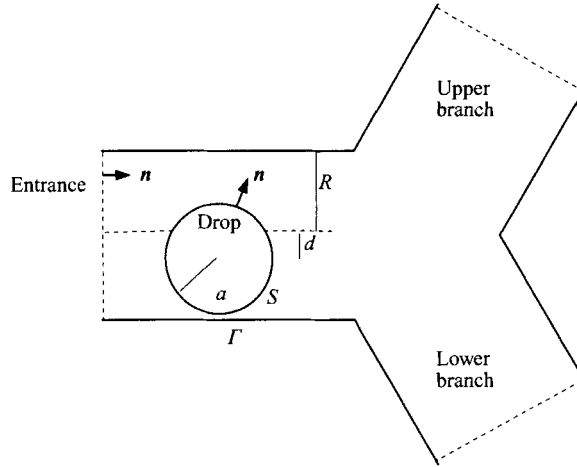
FIGURE 2. Geometry of the model problem.

2. Problem formulation

The geometry of the model problem, consisting of a neutrally buoyant two-dimensional drop with viscosity $\lambda\mu$ in a suspending fluid with viscosity μ, is illustrated in figure 2. We denote the surface of the drop by S and the walls of the bounding tube by Γ. The unit normal n is directed into the suspending fluid, and away from S and Γ. Flow in the drop (volume V_d) and suspending fluid (volume V_s) satisfy Stokes equations

$$\nabla \cdot \boldsymbol{T}_d = \lambda\mu\nabla^2\boldsymbol{u}_d - \nabla p_d = 0 \quad \text{and} \quad \nabla \cdot \boldsymbol{u}_d = 0 \quad \text{for} \quad \boldsymbol{x} \in V_d \tag{2.1}$$

and

$$\nabla \cdot \boldsymbol{T}_s = \mu\nabla^2\boldsymbol{u}_s - \nabla p_s = 0 \quad \text{and} \quad \nabla \cdot \boldsymbol{u}_s = 0 \quad \text{for} \quad \boldsymbol{x} \in V_s \tag{2.2}$$

where the subscripts s and d denote the suspending fluid and dispersed phase, respectively, $\mathbf{u}$ is the fluid velocity, p is the fluid pressure, $\boldsymbol{T}$ is the stress tensor, and $\boldsymbol{x}$ is the position vector. Stokes equations are valid provided the Reynolds number

$$\mathscr{R} = \frac{\rho U R}{\mu} \ll 1 \tag{2.3}$$

where U is a characteristic fluid velocity, R the capillary radius, and ρ the fluid density. The Reynolds number is typically small in geological porous material owing to small pore sizes as well as small fluid velocities.

On the surface of the drop the velocity is continuous,

$$\mathbf{u}_s = \mathbf{u}_d \quad \text{for} \quad \boldsymbol{x} \in S. \tag{2.4}$$

In the model problem considered here, the velocity of the suspending fluid is specified both at the entrance and the exits of the tube shown in figure 2. We impose a parabolic velocity profile, characteristic of Poiseuille flow, at all three orifices. The velocity of the fluid entering the branching tube from the left (see figure 2) is given by

$$\mathbf{u} \cdot \boldsymbol{n} = U\left[1 - \left(\frac{r}{R}\right)^2\right] \tag{2.5}$$

where r is the distance from the tube centreline.

Parameter	Description
a/R	dimensionless drop radius
d/R	dimensionless drop offset from tube centerline
Q	flow through upper branch divided by total flow
λ	viscosity ratio
$\mathscr{C}$	Capillary number, ratio of viscous to interfacial tension stresses

TABLE 1. Dimensionless parameters: lengths are normalized by R and velocities by U (see figure 2).

For a neutrally buoyant drop, the stress jump across the surface of the drop is given by

$$[\![\boldsymbol{n}\cdot\boldsymbol{T}]\!]_d = \boldsymbol{n}\cdot\boldsymbol{T}_s - \boldsymbol{n}\cdot\boldsymbol{T}_d = \sigma\,(\nabla_s\cdot\boldsymbol{n})\boldsymbol{n}, \quad \boldsymbol{x} \in S \tag{2.6}$$

where σ is the interfacial tension which is assumed constant. The effect of surfactants, which leads to an additional tangential component in the stress jump condition that depends on the gradient of interfacial tension, is discussed by Ratulowski & Chang (1990) and Borhan & Mao (1992). Owing to the small length scales which typically characterize the interfaces in the physical problems studied here, surfactant effects will probably play a significant role in actual porous media. Nevertheless, we will neglect the effects of surfactants in this paper. In the physical system, non-hydrodynamic forces due to electrostatic or intermolecular effects typically become important for separation distances less than about 10 nm. The coalescence and breakup of drops cannot be simulated within the continuum mechanics framework studied here.

The characteristic length, velocity and time scales are chosen to be R, U and R/U, respectively. The stress jump is characterized by a capillary number, which represents the ratio of viscous to interfacial tension stresses,

$$\mathscr{C} = \frac{\mu U}{\sigma}. \tag{2.7}$$

In geological porous media, $\mathscr{C}$ is usually smaller than about 0.01. Here we also consider much larger $\mathscr{C}$ which allows for greater drop deformation. For the range of drop sizes studied here, the effects of interfacial tension on the dynamics typically become saturated for capillary numbers based on the drop size $\mathscr{C}_d = \mu U a/\sigma R < O(10^{-1})$.

Flow through the tube is characterized by the flux through the upper branch, Q_{upper}, divided by the flux entering the tube from the left, $Q_{\text{upper}} + Q_{\text{lower}}$, i.e.

$$Q = \frac{Q_{\text{upper}}}{Q_{\text{upper}} + Q_{\text{lower}}}. \tag{2.8}$$

We will assume that the flow rate through the upper branch is always greater than through the lower branch. The dimensionless parameters which characterize the problem are summarized in table 1.

Here we only present results for the specific geometry shown in figure 2. The motion of a single particle depends only 'weakly on the geometry of the bifurcation' (Audet & Olbricht 1987). The effect of changing the relative orientation of the three branches on the partitioning of rigid spheres in dilute suspensions is discussed by Ditchfield & Olbricht (1995). Similarly, the 'sharpness' of the corners of the tube has little effect on the flow but will affect the tractions on the tube walls in the vicinity of the corners (e.g. Higdon 1985).

Stokes equations may be recast as integral equations for the interfacial velocities, $u_d(x)$ for $x \in S$, and the surface tractions, $n \cdot T_s$ for $x \in \Gamma$. The integral representations for the velocity, and associated integral equations for the interfacial velocity and surface traction are given by (e.g. Martinez & Udell 1990)

$$- \int_S [\![n \cdot T]\!]_d \cdot J \, \mathrm{d}S_y - (1-\lambda) \int_S n \cdot K \cdot u_d \, \mathrm{d}S_y - \int_\Gamma n \cdot T_s \cdot J \, \mathrm{d}S_y$$

$$- \int_\Gamma n \cdot K \cdot u_s \, \mathrm{d}S_y = \begin{cases} u_s(x), & x \in \text{suspending fluid}, \\[2mm] \lambda u_d(x), & x \in \text{drop}, \\[2mm] \tfrac{1}{2}(1+\lambda)u_d(x), & x \in S, \\[2mm] c u_s(x), & x \in \Gamma, \end{cases} \qquad (2.9)$$

where c is a function of the smoothness of the boundary. J and K are known two-dimensional kernels for velocity and stress (e.g. Pozrikidis 1992),

$$J = -\frac{1}{4\pi} \left(I \log |x-y| - \frac{(x-y)(x-y)}{|x-y|^2} \right), \quad K = -\frac{(x-y)(x-y)(x-y)}{\pi |x-y|^4} \qquad (2.10)$$

where y is the integration variable.

The interfacial velocity along the surface of the drop and the tractions along the tube walls are determined by solving equations (2.9) using standard numerical collocation procedures. Equations (2.9) are integral equations of the first kind for the tractions on the tube walls, and are thus ill-posed; however, following previous studies (e.g. Borhan & Mao 1992), rather than reformulating (2.9) as equations of the second kind, we simply solve the first-kind equations and verify that we do not have sawtooth-type oscillatory solutions. The unknown velocities are assumed to vary linearly, and the tractions along the wall are assumed to be constant, between collocation points. The singularities in the kernels are subtracted and integrated analytically (see Pozrikidis 1992, pp. 178–180). Some care is necessary near the corners of the tube. Integrations are performed using eight-point Gauss–Legendre quadrature. The drop shape is described by cubic splines parameterized in terms of arclength. The drop is represented by 40–80 evenly spaced collocation points. The tube walls are represented by 270 collocation points which have a higher concentration near corners of the tube. In the numerical calculations, the cross-sectional area of the drop changes by up to 1% over the course of a complete simulation. Eigenfunction deflation (Pozrikidis 1992, pp. 120–124), which would greatly reduce area changes and allow us to consider $\lambda \ll 1$, was not implemented.

The time-dependent motion of the interface is determined using the kinematic condition

$$\frac{\mathrm{d}x}{\mathrm{d}t} = u(x), \qquad x \in S. \qquad (2.11)$$

Equations (2.11) are solved using a second-order Runge–Kutta method. Owing to the very large differences between the timescale of interfacial-tension-driven motions for $\mathscr{C} \ll 1$ and the pressure-driven flow, equations (2.11) are stiff, and we are limited to considering $\mathscr{C} > 0.01$.

Finally, we note that since the drops studied here are deformable and can thus migrate across streamlines, the initial upstream position of the drop will affect their

trajectory. Specifically, analytical results for a three-dimensional drop in a two-dimensional Poiseuille flow (Chan & Leal 1979) indicate that the drop will migrate towards the tube centreline for $\lambda < 0.5$ and $\lambda > 10$, but towards the wall for $0.5 < \lambda < 10$. Numerical calculations by Zhou & Pozrikidis (1994) indicate that drops migrate towards the tube centreline for $\lambda < O(1-10)$ depending on the position of the drops; otherwise, there appears to be an equilibrium position for no migration. Experimental observations (W. L. Olbricht, personal communication) also show that moderate-viscosity-ratio three-dimensional drops migrate to an off-axis equilibrium position. Thus, in addition to the five parameters listed in table 1, we could introduce a second geometrical parameter which describes the initial upstream position of the drop. In the simulations presented here, the drops are assumed to be initially circular and located approximately $4R$ upstream from the bifurcation. This assumption is made for two reasons:

(i) The branching tube model (figure 1) simulates the presence of bifurcations in a porous material, and for many materials the distance between bifurcations will be $O(R)$.

(ii) The (normalized) timescale for the drop to deform is $O(a(1 + \lambda)\mathscr{C}/R)$ which is $< O(1)$ for the calculations presented here, so that the drops deform to their nearly steady shape before they have translated more than about one drop radius, and well before they reach the bifurcation. The rapid deformation compared to advection is most clearly seen in animated videos.

Since the rate of migration due to deformation is small, the initial upstream position has a negligible effect provided the distance from the bifurcation is $> O(R)$. As a result, the dynamics can be characterized by a single geometrical parameter describing the initial conditions, i.e. d/R.

3. Results

The model problem is described by the five dimensionless parameters listed in §2 and table 1. Here we consider the effects of each of the parameters on the motion of a single drop. In figures 3, 4 and 5 we show sequences of drop shapes which illustrate the effects of changing the viscosity ratio, capillary number and drop size, respectively. In figure 6 we summarize a large of number of calculations of the dynamics of a single drop. We characterize the behaviour of the drops (i.e. which branch they pass through) by the initial position of the centre of mass of the drop which separates trajectories passing through the upper and lower branches. The motion of drops of finite size can be compared with the behaviour of a passive tracer (i.e. an infinitesimally small drop).

In figure 3 we show two calculations for the same initial configuration and imposed flow, and vary only the viscosity ratio; $a/R = 0.5$, $Q = 0.75$, $\mathscr{C} = 0.5$ and $d/R = 0.4$. The drop with $\lambda = 0.1$ (which we will refer to as a bubble) passes through the upper branch whereas the drop with $\lambda = 5$ passes through the lower branch. Notice that the drops are deformed by the flow (e.g. shapes at $t = 2$) and as a result can migrate from the region of high shear (near the wall) to low shear (near the tube centreline) for sufficiently low viscosity ratios (Chan & Leal 1979). The bubble enters the upper branch since it translates more rapidly away from the wall and is able to pass around the bifurcation. For sufficiently large viscosity ratios, the drop will not migrate away from the wall (Zhou & Pozrikidis 1994). The higher-viscosity-ratio drop will also move normal to the wall more slowly due to greater lubrication forces associated with
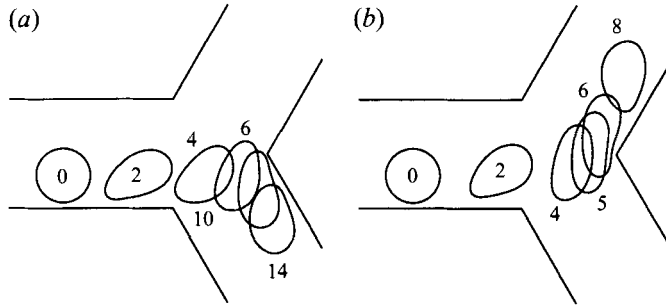
FIGURE 3. Effect of the viscosity ratio: (*a*) $\lambda = 5$ and (*b*) $\lambda = 0.1$; $a/R = 0.5$, $Q = 0.75$, $\mathscr{C} = 0.5$, $d/R = 0.4$. Times are labelled next to the corresponding drop shape.
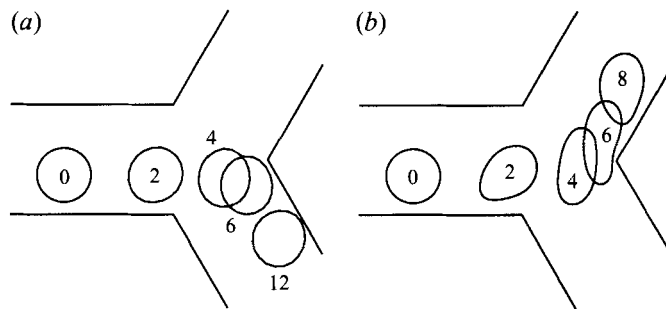

FIGURE 4. Effect of the capillary number: (*a*) $\mathscr{C} = 0.1$ and (*b*) $\mathscr{C} = 0.5$; $a/R = 0.5$, $Q = 0.7$, $\lambda = 0.1$, $d/R = 0.3$. Times are labelled next to the corresponding drop shape.
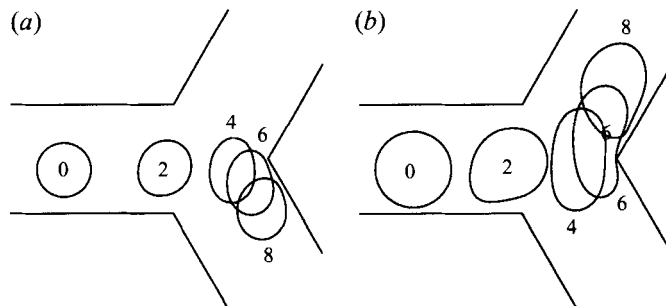

FIGURE 5. Effect of drop size: (*a*) $a/R = 0.5$ and (*b*) $a/R = 0.7$; $\lambda = 0.1$, $Q = 0.6$, $\mathscr{C} = 0.25$, $d = 0.2$. Times are labelled next to the corresponding drop shape.

the small gap between the drop and the wall. For comparison, in figure 6 shown later, we will see that passive tracers at positions $d/R > 0.347$ will enter the lower branch.

In figure 4 we show two calculations for the same initial conditions and viscosity ratio, and vary only the capillary number; $a/R = 0.5$, $Q = 0.7$, $d/R = 0.3$ and $\lambda = 0.1$ (bubble). The $\mathscr{C} = 0.1$ bubble remains nearly spherical, whereas the $\mathscr{C} = 0.5$ bubble becomes deformed, drifts away from the wall, and can thus pass around the bifurcation. For comparison, passive tracers at positions $d/R > 0.273$ will enter the lower branch.

In figure 5 we consider the effect of drop size. We show two calculations for different bubble sizes but with their centres of mass initially at the same position; $Q = 0.6$,
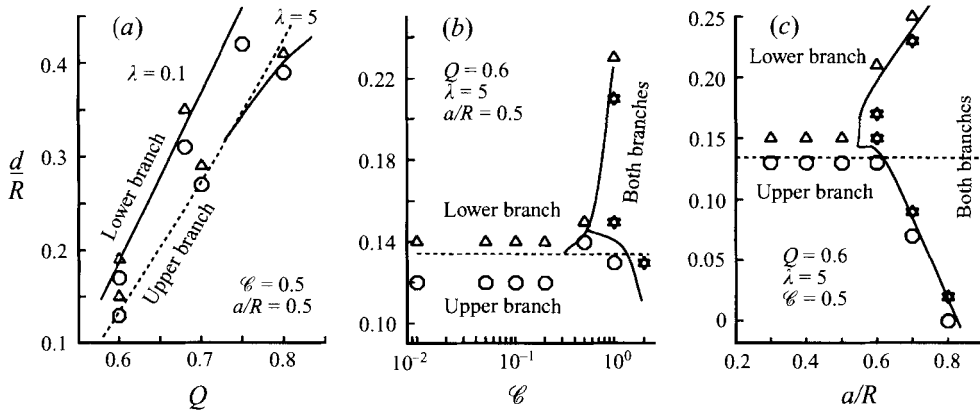
FIGURE 6. Effect of (a) viscosity ratio, λ, and flow partitioning, Q, (b) capillary number, $\mathscr{C}$, and (c) drop size, a/R, on drop behaviour. Dynamics are characterized for a given initial position d/R by whether the drop enters the upper branch (open circle), the lower branch (open triangle) or is stretched down both downstream branches (star). The dashed curves represent the position of the streamline which separates fluid that enters the upper and lower branches in the absence of a drop.

$\mathscr{C} = 0.25$, $d/R = 0.2$ and $\lambda = 0.1$ (bubble). The smaller bubble enters the lower branch whereas the larger bubble enters the upper branch. Again, the larger bubble can migrate more rapidly owing to its greater deformation (here the capillary number is based on the tube radius, not the drop size) and can enter the upper branch; for comparison, passive tracers at positions $d/R > 0.134$ will enter the lower branch.

The effects of the different parameters characterizing the motion of a single drop are summarized in figure 6. We present the results of nearly 100 simulations to determine the initial position of drops which separate trajectories that enter the upper and lower branches (referred to hereafter as the critical drop offset). Since most of the results presented in figures 3–5 are for $\lambda = 0.1$ we focus on $\lambda = 5$ in figures 6(b–c). Simulations in which the drop enters the upper branch are shown with an open circle, whereas drops entering the lower branch are denoted by an open triangle. For comparison, the position of the streamline separating flow into the upper and lower branches in the absence of a drop is shown with a dashed line.

As illustrated in figure 3, and figure 6(a), as the viscosity ratio λ decreases, the critical drop offset d/R increases. Thus, bubbles have a particularly strong tendency to follow the high-flow-rate pathway. In the numerical calculations for large capillary numbers or drop sizes (typically for capillary numbers based on the drop radius $\mathscr{C}_d > 0.3$) we observed cases in which the drop is stretched at the bifurcation and would be carried down both branches; in a three-dimensional capillary we expect that the drop would eventually break up. The flow near the bifurcation resembles (qualitatively) an extensional flow and the dynamics of the drops in the vicinity of the bifurcation are similar to drops in extensional flows. In particular, for $\mathscr{C}_d$ greater than some critical value (about 0.3), drops are stretched down both branches for all viscosity ratios just as drops are elongated indefinitely in extensional (but not shear) flows for $\mathscr{C}$ greater than the critical capillary number (e.g. Stone 1994).

Finally we note that the drops slow down in the vicinity of the bifurcation, as is evident in figures 3–5, since the drop is affected by the competing flows through the upper and lower branches which leads to the formation of a stagnation point at the bifurcation. The velocity of the drops once they have passed the bifurcation is also typically reduced (compared to the free-stream velocity) since the drops end up closer
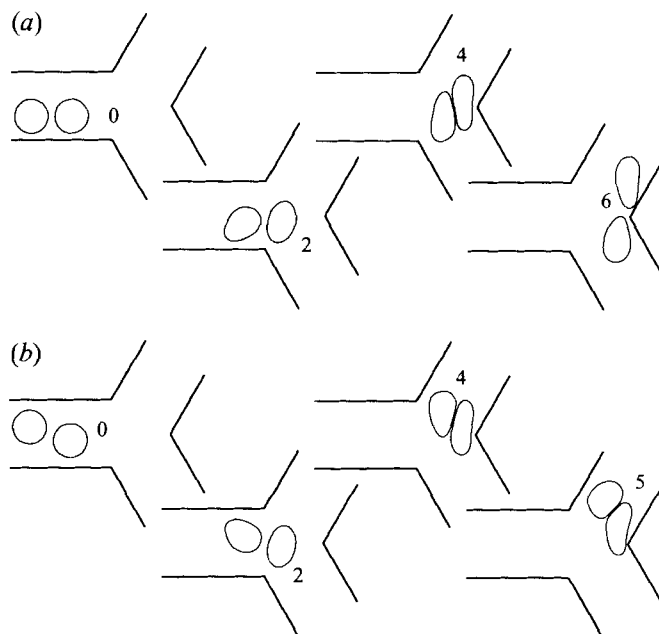
FIGURE 7. Effect of hydrodynamic interactions: (a) $d/R = 0.3$ and (b) $d/R = \pm 0.2$; $\lambda = 0.1$ (bubble), $Q = 0.7$, $\mathscr{C} = 0.5$, $a/R = 0.5$. Times are labelled next to the corresponding bubble shape. The sequence in (a) should be compared with figure 4(b).

to a wall. In the next section we will study some of the consequences of the reduction in translation speed.

4. Drop interactions

The results presented in §3 are relevant to the limit of very dilute suspensions. Here we consider the effects of the interactions between two drops on their motion through the branched tube. Again we employ the boundary integral method to study the problem numerically. Equations (2.9) can be modified in a straightforward manner to study the additional drop (e.g. Manga & Stone 1993, Appendix A). Below we present two sequences of drop shapes which illustrate qualitatively two different effects of drop interactions.

In figure 7(a) we show a sequence of bubble shapes in which the leading bubble ($\lambda = 0.1$) enters the upper branch whereas the second bubble enters the lower branch. For comparison a single bubble with the same initial vertical position enters the upper branch (see figure 4b). As the first bubble approaches the bifurcation its translation speed is reduced and the second one finds the upper branch partially 'blocked' (i.e. the second bubble is being pushed by the flow from behind but resisted by the presence of the first bubble in the front) and is carried around the first bubble and into the lower branch. Ditchfield & Olbricht (1995) have studied experimentally this type of phenomenon in more detail and found that for volume fractions of solid particles greater than about 2%, hydrodynamic interactions between the suspended particles affect their partitioning at bifurcations.

In the second simulation, presented in figure 7(b), the trailing bubble is carried around the first one as the bubbles pass by the bifurcation. This type of interaction
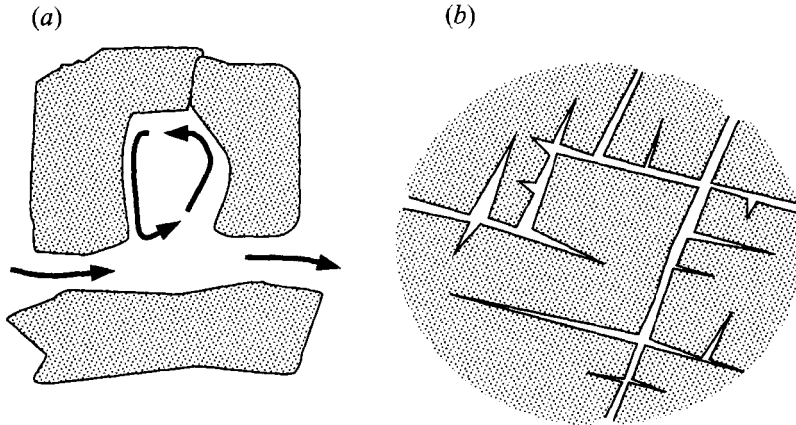
FIGURE 8. Schematic illustration of dead-end pores in (a) granular and (b) fractured porous materials.

also arises due to the reduction in translation speed of the leading bubble as it approaches the bifurcation. For drops smaller than the tube radius, the relative positions and orientations of the drops can change as the drops pass bifurcations; such motions will increase cross-stream transport from the capillary walls to the free stream and vice versa. Thus, the presence of a dispersed phase should enhance mixing and reactions between the fluid and porous medium by inducing lateral and time-dependent fluid motions.

5. 'Cleaning' porous materials using suspensions

Many porous media, including granular and fractured materials (see figure 8), contain dead-end pores. Contaminants may be contained within the fluid in the pore or adsorbed on the surface of the pore. If a clean or desorbing fluid is released into the porous material, it will be unable to flow into such dead-end pores, as illustrated in figure 9(a) where we show calculated streamlines inside a cavity which represents the dead-end pore. Inside the cavity there is a recirculating flow which is isolated from the free stream so that transfer into the cavity will be limited by molecular diffusion. For a discussion of cavity flows, the reader is referred to Moffatt (1964) who studied flow in a corner, and Higdon (1985, 1990) who presented solutions for flow over cavities of various shapes and dimensions.

The presence of a dispersed phase in the porous medium will affect the local flow in a time-dependent manner as drops pass over the pore. For example, in figure 9(b) we show calculated streamlines as a drop passes over the pore. A comparison of the flow in the presence of the drop (figure 9b) with the flow in the absence of the drop (figure 9a) illustrates the time-dependence of the cavity flow as the drop passes over the cavity. Thus, the motion of the drop allows fluid transfer between the free stream and the dead-end pore.†

The effect of different characteristics of the dispersed phase on the amount of transfer between the free stream and dead-end pore is illustrated in figure 10. In order to quantify the 'cleaning' process, we calculate the advection of the (numerically

† The idea of using suspensions to clean 'dead-end' pores is attributed to discussions with H. A. Stone from Harvard University.
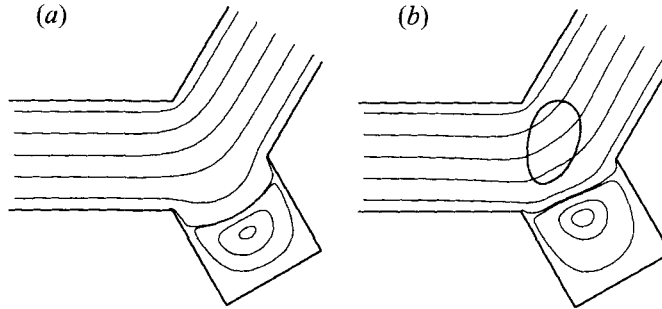
FIGURE 9. Calculated streamlines (a) in the absence of a drop and (b) when the drop ($\lambda = 1$ and $\mathscr{C} = 0.5$) is above the dead-end pore. The disturbance created by the drop results in a flow which depends on the position of the drop and thus allows fluid transfer between the pore and free stream.
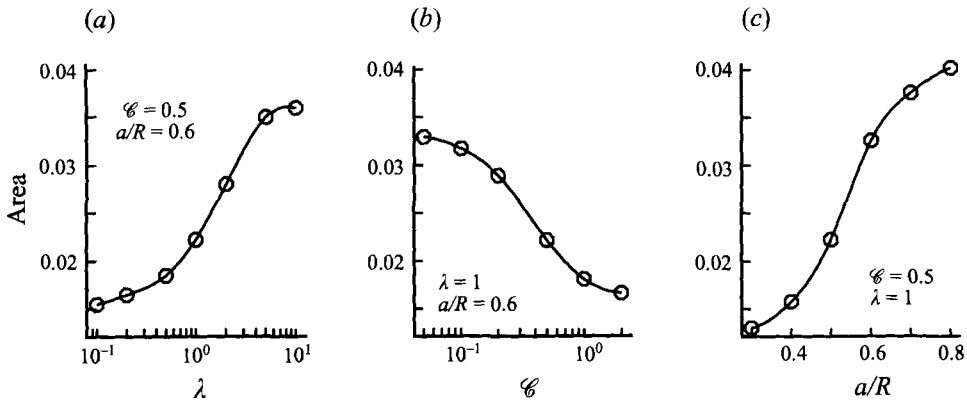

FIGURE 10. The effect of (a) viscosity ratio, λ, (b) capillary number, $\mathscr{C}$, and (c) drop size, a/R, on the area (normalized by R^2) of fluid transferred between the pore and the free stream.

calculated) material line which initially separates the fluid trapped in the 'dead-end' pore from fluid in the free stream (see figure 9a). Once the drop has passed over the pore we calculate the area of fluid which has been entrained into the pore. In figure 10 we show the area of fluid transferred as a function of the viscosity ratio, capillary number and drop size. As expected, drops with high viscosity ratios, small capillary numbers and large sizes are more effective at cleaning the pore since they have a larger effect on the disturbance flow. Since fluid velocities inside the pore are much smaller than the free-stream velocities (typically one or two orders of magnitude smaller), the area of fluid entrained into the pore is only a few percent of the area of the drop so that cleaning a pore would require hundreds of drops. Nevertheless, transport induced by drops is likely to be more effective than molecular diffusion alone which limits transfer in the absence of a dispersed phase.

6. Summary

The extension of the pore-scale results presented here to the determination of macroscopic physical properties is not straightforward. In particular, we are limited by the two-dimensional geometry assumed in the calculations, the simplification of the pore geometry, and the constant-flow-rate (as opposed to constant-pressure) boundary

conditions. We have also only considered the limit in which the undeformed diameter of the drop is less than the tube diameter. Nevertheless, in this summary we attempt to qualitatively relate the results presented in §§3 and 4 to macroscopic quantities.

If we can characterize the dispersion of the dispersed phase (i.e. mechanical spreading) by the likelihood of the drop entering the lower-flow-rate channel, then we infer based on the results presented in §3 that dispersion decreases as drop viscosity ratio decreases, as the capillary number increases and as the drop size increases. The results presented in §3 show that the suspended phase has a strong tendency to follow high-flow-rate channels. Thus, the presence of a dispersed phase in a heterogeneous porous material will change the distribution of 'effective' permeability due to spatially varying concentrations of the dispersed phase. Specifically, we expect that the concentration of the dispersed into high-flow-rate channels (regions with high permeabilities) will decrease the effective permeability of such regions.

From the two-drop simulations we infer that mechanical dispersion increases as the concentration of the dispersed phase increases owing to the interactions between the drops near the bifurcation. The results presented in §4 also suggest that the presence of a dispersed phase should enhance mixing and diffusive transfer between the walls and suspending fluid by inducing lateral and time-dependent fluid motions.

Finally, we demonstrated that the motion of a drop over a 'dead-end' pore allows fluid transfer between the pore and free stream and thus the use of suspensions may improve the efficiency of cleaning porous materials. An experimental study of such cleaning processes is being developed currently. The effects of a dispersed phase on fluid transfer between the free stream and the cavity may have applications to related problems, for example flow over rough reacting surfaces, in which reaction products and byproducts may trapped inside cavities on the surface.

REFERENCES

ADLER, P. M. 1992 *Porous Media: Geometry and Transports.* Butterworth-Heinemann.
AUDET, D. M. & OLBRICHT, W. L. 1987 The motion of model cells at capillary bifurcations. *Microvascular Res.* 33, 377–396.
BORHAN, A. & MAO, C. F. 1992 Effect of surfactants on the motion of drops through circular tubes. *Phys. Fluids* A 4, 2628–2640.
BRENNER, H. 1971 Pressure drop due to the motion of neutrally buoyant particles in duct flows. II. Spherical droplets and bubbles. *Indust. Engng Chem. Fundam.* 10, 537–543.
BRETHERTON, F. P. 1961 The motion of long bubbles in tubes. *J. Fluid Mech.* 10, 166–188.
CHAN, P. H. & LEAL, L. G. 1979 The motion of a deformable drop in a second order fluid. *J. Fluid Mech.* 92, 131–170.
DITCHFIELD, R. & OLBRICHT, W. L. 1995 Effects of particle concentration on the partitioning of suspensions at small divergent bifurcations. Manuscript in review.
GUNSTENSEN, A. K. & ROTHMAN, D. H. 1993 Lattice-Boltzmann studies of immiscible two-phase flow through porous media. *J. Geophys. Res.* 98, 6431–6441.
HIGDON, J. J. L. 1985 Stokes flow in arbitrary two-dimensional domains: Shear flow over ridges and cavities. *J. Fluid Mech.* 159, 195–226.
HIGDON, J. J. L. 1990 Effect of pressure gradients on Stokes flows over cavities. *Phys. Fluids.* A 2, 112–114.
HO, B. P. & LEAL, L. G. 1975 The creeping motion of liquid drops through a circular tube of comparable diameter. *J. Fluid Mech.* 71, 361–384.
HYMAN, W. A. & SKALAK, R. 1972 Viscous flow of a suspension of liquid drops in a cylindrical tube. *Appl. Sci. Res.* 26, 27–52.

MANGA, M. & STONE, H. A. 1993 Buoyancy-driven interactions between two deformable viscous drops. *J. Fluid Mech.* **256**, 647–683.

MARTINEZ, M. J. & UDELL, K. S. 1990 Axisymmetric creeping motion of drops through circular tubes. *J. Fluid Mech.* **210**, 565–591.

MOFFATT, H. K. 1964 Viscous and resistive eddies near a sharp corner. *J. Fluid Mech.* **18**, 1–19.

POZRIKIDIS, C. 1992 *Boundary Integral and Singularity Methods for Linearized Viscous Flow.* Cambridge University Press.

RATULOWSKI, J. & CHANG, H.-C. 1989 Transport of gas bubbles in capillaries. *Phys. Fluids* A **1**, 1642–1655.

RATULOWSKI, J. & CHANG, H.-C. 1990 Marangoni effects of trace impurities on the motion of long gas bubbles in capillaries. *J. Fluid Mech.* **210**, 303–328.

STONE, H. A. 1994 Dynamics of drop deformation and breakup in viscous fluids. *Ann. Rev. Fluid Mech.* **26**, 65–102.

TSAI, T. M. & MIKSIS, M. J. 1994 Dynamics of a drop in a constricted capillary tube. *J. Fluid Mech.* **274**, 197–217.

ZHOU, H. & POZRIKIDIS, C. 1994 Pressure-driven flow of suspensions of liquid drops. *Phys. Fluids* **6**, 80–94.